Investigation of Arc Force Effects in Subsurface GTA Welding

The force exerted by the welding arc plasma jet generally follows a parabolic relationship with the welding current and increases with an increase in electrode immersion depth

BY Y. ADONYI, R. W. RICHARDSON AND W. A. BAESLACK III

ABSTRACT. The force exerted by the gas tungsten arc (GTA) plasma jet has been measured using a weighing method for both surface and subsurface welding conditions. The effects of welding current, electrode tip position relative to the surface of the workpiece, base metal type, and shielding gas on arc force have been experimentally determined. Results obtained for surface GTA welds showed the arc force to increase with welding current between 100 and 800 A by a parabolic relationship, which is consistent with experimental results obtained by most previous investigators and supported by theory. Surface arc force measurements for both titanium and stainless steel alloy base metals and a water-cooled copper anode also showed that the arc force increases with a decrease in the electrode tip-to-workpiece distance and, for identical welding conditions, to be higher for welds produced with argon vs. helium. In addition, higher levels of arc force were measured for welds produced in titanium vs. stainless steel for identical welding parameters. Submersion of the electrode tip to depths of 2 and 4 mm below the workpiece surface promoted an increase in the arc force. As with surface measurements, the arc force increased parabolically with welding current and was higher for welds produced with argon vs. helium for all other conditions being identical. In contrast to the surface condition, higher levels of arc force were recorded for stainless steel vs. titanium. Arc force measurements performed on the water-cooled copper anode indicated that a geometric containment effect, which influences the transfer of momentum from the plasma jet to the anode surface, contributes in part to the higher arc force measured in the subsurface vs. the surface conditions.

Y. ADONYI is a Sr. Research Engineer, USS, a Division of USX Corp., Technical Center, Monroeville, Pa. R. W. RICHARDSON and W. A. BAESLACK III are Associate Professor and Professor, respectively, Department of Welding Engineering, The Ohio State University, Columbus, Ohio.

Introduction

Subsurface Gas Tungsten Arc Welding

Subsurface gas tungsten arc (GTA) welding, which is commonly known as "immersed" or "buried arc" GTA welding, is a variation of conventional GTA welding, which effectively extends the process to the joining of thick materials (Refs. 1–18). In subsurface GTA welding, the tip of the nonconsumable tungsten electrode is gradually submerged below the surface of the workpiece. Through the use of high welding currents (typically between 500 and 1000 A), a high arc force is generated, which promotes formation of a deep cavity in the molten weld pool within which the end of the electrode may be immersed. This electrode condition effectively localizes the heat source nearer to the plate center and increases the heat transfer efficiency by reducing radiation losses.

KEY WORDS

Welding Arc
Arc Force Effects
Submerged Arc GTAW
Immersed Electrode
Helium vs. Argon
Arc Plasma Jet
Base Metal Effects
Shielding Gas Effects
Martensitic Stainless
Titanium

Figure 1 defines the specific elements and terminology associated with the immersed arc GTA welding process. Note the large electrode diameter, electrode tip immersion depth (which may exceed tens of millimeters at high current levels) and large pool cavity.

The stability of the subsurface GTAW process is dependent on the establishment of equilibrium between the force of the arc plasma jet exerted upon the weld pool surface and the hydrostatic and surface tension forces associated with the displaced molten metal. This arc force, which equals the arc pressure integrated over the area of the arc at the anode, results from the transfer of momentum from the plasma jet to the weld pool surface. While this force balance is maintained, the process remains stable. However, if these forces become unbalanced, weld discontinuities may form such as cavities at the weld root, or total process instability may result.

Considering this prerequisite force balance, it is apparent that the process is most suitable for joining low-density alloys, as an equivalent arc force or pressure can displace a greater volume of liquid and thereby allow deeper electrode immersion and greater fusion zone penetration. Similarly, alloys exhibiting a low thermal conductivity are also most amenable to the process, as this physical property promotes a greater concentration of the welding heat, *i.e.*, a higher melting efficiency.

Origin of Arc Force in GTA Welding

Arc force originates from the action of the arc plasma jet impinging upon the

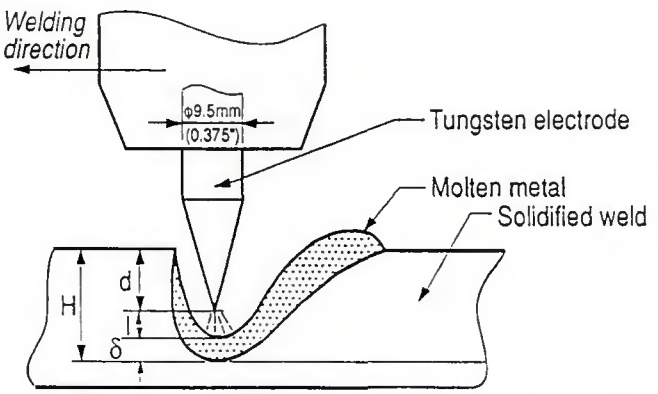

Fig. 1 — Schematic illustration showing longitudinal cross-section through subsurface GTA weld. Electrode tip immersion depth is d; the molten metal thickness below the arc is d; true arc length is l; and the total fusion zone penetration depth is H.

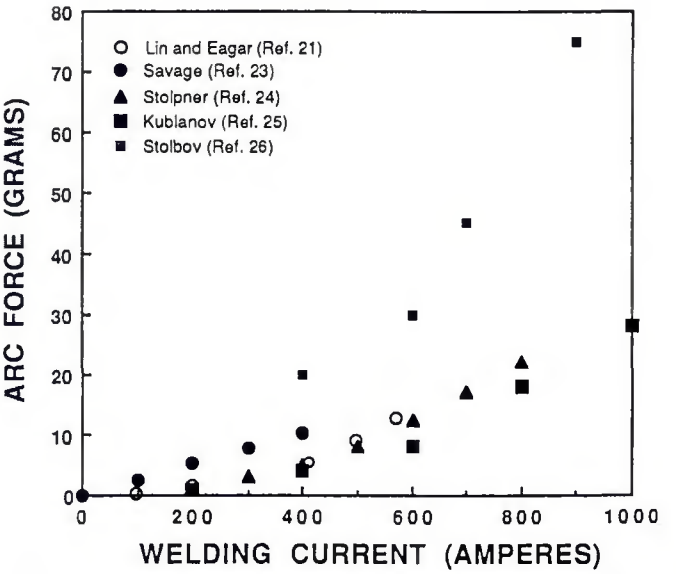

Fig. 2 — Plot of arc force vs. welding current for surface arc GTA welds (Refs. 21, 23–26). Data by Lin and Eagar (Ref. 21) is integrated arc force determined from arc pressure measurements. Data by Savage, et al. (Ref. 23), and Stolbov (Ref. 26) is total ("uncorrected") arc force. Kublanov and Erokin (Ref. 25) is for plasma jet (i.e., corrected).

weld pool surface (*i.e.*, the stagnation pressure) (Refs. 19–21). During GTA welding, current flows through a conductor of ionized shielding gas, thereby generating a self-induced magnetic field circumferentially around the arc. The interaction between the current flow and this magnetic field produces a (J X B) Lorentz force in a direction toward the central, longitudinal axis of the arc. The radial constriction caused by the Lorentz force is balanced by a radial pressure gradient in the arc. In a typical GTA welding arc produced under direct current, electrode negative conditions, natural constriction occurs at the cathode spot located on the tip of the tungsten electrode, thereby promoting a divergent current distribution (*e.g.*, a Gaussian distribution). Since the current density at the cathode is greater than at the anode, the cathode region exhibits a higher gas pressure than the unconstricted anode region. This difference in static plasma pressure results in the creation of a plasma jet from the cathodic tungsten electrode to the anodic weld pool surface. As indicated above, the arc force, or pressure, is associated with the transfer of momentum from this plasma jet to the weld pool surface.

Measurement of Arc Force and Parametric Effects

Arc force measurement data presented in the published literature are limited to the conventional surface GTA welding process. Basically, two methods have been employed to measure arc force: "weighing" and "pressure" methods. Weighing methods involve the use of scales or balances in which the deflection of the base plate or nonconsumable anode is precisely measured and related to the arc force. The measurement of arc pressure is generally more complex and involves the welding on a thin plate containing a fine hole, or alternatively, the insertion of an appropriate probe into the plasma jet. The advantage of such pressure measurements over weighing methods is that they allow characterization of the arc pressure distribution. Integration of the measured arc pressure over the area of the arc provides the value of the arc force generated by the arc plasma jet.

As reviewed by Erokhin (Ref. 22), numerous investigators have experimentally measured the arc force exerted for both consumable and nonconsumable electrode welding processes. With few exceptions, most investigators generally agree that the arc force is related to the welding current by the following parabolic relationship:

$$F_{arc} = kI^2 \qquad (1)$$

where I = welding current and k is a constant dependent on the tungsten electrode tip geometry, arc length, anode material, etc. In his review, Erokhin (Ref. 22) compared the results of 33 different authors and found k values to range from about 5 to 6 X 10^{-6} g/A^2 in the 100- to 300-A range. These values were obtained from measurements of the total arc force, which included contributions of both the plasma-jet force and three-dimensional electromagnetic volumetric forces on the weld pool.

Figure 2 provides a summary of data obtained from the published literature for surface GTA welds (Refs. 21, 23–26). Although a parabolic relationship between arc force and arc current was generally observed, which is consistent with theory, a wide range of absolute force values have been obtained. The only exception is the work of Savage and coworkers (Ref. 24), who observed a linear relationship between the arc force and current. These differences result in part from the use of different experimental apparatus, the measurement of total vs. corrected arc force, differences in the manner in which correction factors were determined, and finally, from the variation in process parameters and conditions other than exclusively welding current.

Ultimately, the goal of characterizing the arc force during GTA welding is to relate measured values to the welding process performance, the weld fusion zone surface quality, bead profile and associated defects (humping bead formation, underfill, undercut, void, or cavity formation) and the geometry of the fusion zone cross-section (in particular, the depth of penetration). Clearly, the complex interaction of many additional factors influences these weld characteristics, such as weld metal density, viscosity, electromagnetic (Lorentz) induced volumetric forces, and surface tension driven fluid flow. However, in the specific case of the subsurface GTA

welding process, the arc force plays a critical and dominant role in determining the formation and geometry of the weld pool and fusion zone and in controlling overall process performance.

Objectives

The overall purpose of this study was to investigate the nature of arc force effects in GTA welds produced below the surface. Specific objectives for the study included: 1) evaluating the influence of welding parameters and conditions on arc force measured for conventional, surface GTA weldments; 2) systematically determining the relationships between arc force and pertinent subsurface GTA welding parameters including welding current, electrode tip immersion depth, material type, and shielding gas; 3) relating the arc force measurements to weld pool penetration and geometry.

Experimental Procedure

The Subsurface GTA Welding System

A principal limitation to the effective application of subsurface GTA welding, particularly at high welding currents and travel rates, is a narrow parameter operational range and, correspondingly, a necessity for the accurate control and maintenance of welding parameters. In addition to precise weld parameter control, a requirement of the present investigation included the simultaneous and accurate monitoring of numerous welding system parameters. Both of these goals were achieved through the integration of state-of-the-art welding power and control subsystems into a microcomputer-based control and data-acquisition system.

Two SCR-controlled Miller Intelliweld 650 welding power supplies were connected in parallel to provide a total maximum welding current capability in excess of 1300 A. A D&F Specialties high-current GTA welding torch was used with a Jetline ALC 101 automatic voltage control. Transverse motion of the welding torch was provided by a conventional side beam carriage and a Minarik Model RG-101-UC motor controller. Through the use of a digital-to-analog (D/A) conversion board and output isolators, pertinent welding parameters such as welding current, travel rate, arc voltage and torch position could be automatically and precisely controlled. The use of an analog-to-digital conversion board and input isolators allowed the simultaneous monitoring of pertinent welding parameters and signals, including the actual welding current and voltage. A linear-variable-differential transducer (LVDT) was attached to the welding torch in order to continuously monitor electrode tip position relative to the plate surface.

Each element of the welding system was considered as an individual block and calibrated separately. The static sensitivity and linear attributes of each subsystem were determined and later employed when writing computer programs for the welding schedules.

Arc Force Measurements

Arc force measurements were performed using a weighing method. Although the use of balance beam methods was considered, it was determined that use of a high-resolution commercial scale would instead provide acceptable accuracy, considering the high current and arc forces evaluated in this study, while effectively eliminating electromagnetic disturbances which had caused significant difficulties in several previous studies. A Toledo Scale Model 6112 equipped with a digital strain gauge load cell was used with a Model 8520 signal processor for all arc force measurements. Following signal processing, the information was stored in the microcomputer. An important advantage of this system was its excellent shielding from electromagnetic noise because of the analog/digital signal conversion occurring inside the shielded load cell. Signal transmission and processing were digital, so the signal remained essentially free of noise despite the passage of currents up to 900 A at a distance of only 50 mm (2 in.) from the Wheatstone bridge in the load cell. High-frequency/high-voltage signals used for arc initiation did not influence the scale output.

Numerous sources of error can influence arc force measurements, including electromagnetically induced volumetric forces on the weld pool and surrounding material, electromagnetically induced forces due to welding cables, shielding gas effects, thermal gradients, vibration, and pool oscillation. During all welding experiments, the influence of these effects was minimized by the appropriate positioning of welding cables and use of multiple, symmetric ground connections. To assure accurate force measurements and eliminate extraneous signals in the arc force measurement (isolating on the plasma-jet force), various calibration tests were performed. These procedures included: scale calibration using static weights, welding current calibration using a no-arc condition with a liquid gallium contact and shielding gas/no-arc calibration.

Scale calibration for the maximum load/resolution combination using standard test weights between 0.5 g and 10 kg (0.016 oz and 22 lb) was performed using recommended procedures provided by the scale manufacturer. The use of digital filters helped produce smooth, noise-free output signals following an initial transient period. A resolution of 0.5 g was achieved, which was excellent considering that, with the total weight of the weld specimens and cables, the scale was operating near its mid-range of about 5000 g. Initial transients varied from about 1.2 to 2.0 s, and data collected during these transients were disregarded. Welds were produced for 5 to 10 s after reaching apparent quasi-stationary, steady-state thermal conditions (based on achievement of a constant bead width). Therefore, at a 50-Hz sampling rate, appreciable data points were obtained for averaging a single arc force value.

Eliminating signals other than those resulting from the force of the plasma jet was achieved by measuring the arc force for a current-but-no-arc condition (Ref. 27). For this analysis, the thoriated tungsten electrode was immersed in liquid gallium, and the welding current was varied between 100 to 1200 A in 100 A increments. The no-arc forces were subsequently subtracted from the total arc force measured by the scale during welding.

Measurement of shielding gas effects revealed that the total gas flow pressure was below 0.5 g for argon and helium shielding gases. The influence of the gas flow on arc force measurements was eliminated by zeroing the force reading from the scale, initiating the gas flow, and subsequently zeroing the force reading prior to arc initiation.

Arc Force Measurement Procedures and Test Program

Arc force measurements were performed for both surface and subsurface GTA welding. Variables for tests performed on consumable base materials included base material type, electrode tip position relative to the base plate, and shielding gas. Tests were also performed on a flat, water-cooled copper anode to evaluate changes in the arc force and plasma geometry with welding current and shielding gas. Additional tests were performed on grooved water-cooled copper anodes in order to study the influence of anode geometry (flat vs. grooved to simulate confinement of the arc within a cavity) on arc force.

Materials

Two different base metals were utilized in the present investigation: a Ti-

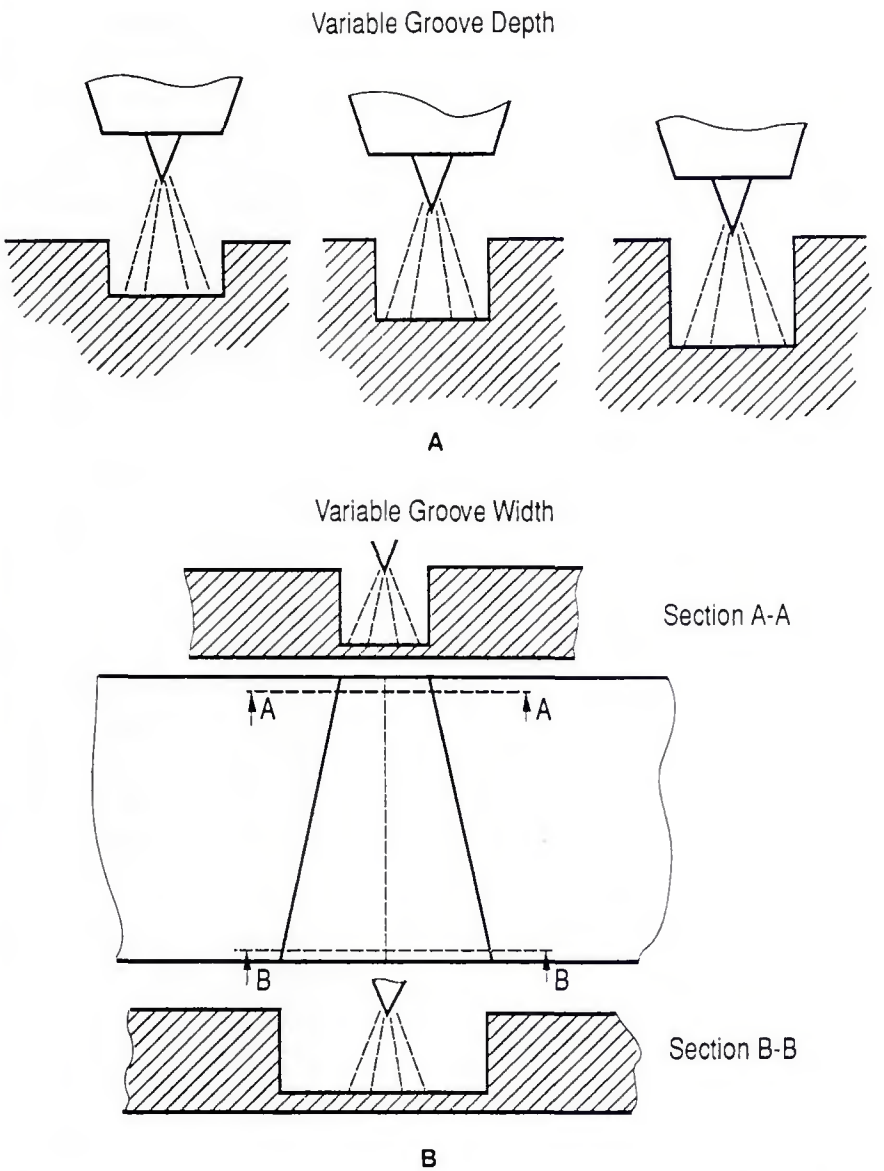

Fig. 3 — Groove geometries for copper anode subsurface GTA simulation experiments. A — Variable groove depth; B — variable groove width.

15V-3Al-3Sn-3Cr (wt-%, hereafter designated as Ti-15-3) titanium alloy and Type 410 martensitic stainless steel. Ti-15-3, which is a metastable beta titanium alloy, was provided in the form of 25.4-mm-thick (1-in.) alpha/beta annealed plate. It was anticipated that the higher beta stabilizer content of this alloy, as compared to conventional alpha/beta titanium alloys, would promote retention of beta phase in the fusion zone on weld cooling, thereby allowing resolution of the solidification grain and subgrain growth structures. Type 410 stainless steel plate 12.7 mm (½ in.) thick was provided in the quenched-and-tempered condition. Fusion zone solidification of this alloy to coarse, columnar ferrite grains allowed resolution of macroscopic solidification behavior experienced by the weld pool.

Surface GTA Welding Measurements

Initial arc force measurement experiments were performed for conventional surface GTA welds to provide a database with which arc force values obtained by previous investigators could be comparatively evaluated and with which subsequently developed data for the subsurface GTAW condition could be compared. All experiments were conducted on 300-mm long by 50-mm wide (12 X 2-in.) plates sectioned from each base material. All welds produced in this program were performed using direct current with the electrode negative (straight polarity). For the surface welding condition, a constant distance of 6 mm (0.24 in.) (the automatic arc voltage controller was deactivated) was maintained between a 9.5-mm (0.37-in.) diameter, 2% thoriated tungsten electrode and the workpiece. The electrode tip included angle was maintained at 30 deg, and the welding current was varied from 100 to 800 A in 100-A increments. Travel rates were also maintained constant at 5.1 mm/s (12 in./min) for each respective base material during these tests (bead width/pool size compensation was not maintained). Consequently, as the welding current was increased, the total energy input into the weld pool, and therefore the weld pool size, increased (assuming only relatively small changes in arc voltage as well as in the arc and melting efficiencies). This methodology was consistent with that used most frequently by previous investigators. Since the welds were performed autogenously (*i.e.*, no filler metal), all welds produced over this wide range of energy inputs did not exhibit complete weld integrity, particularly with regard to the occurrence of an irregular weld surface profile and undercut. Shielding of the welds was provided by argon (38 L/min — 18 ft^3/h) or helium (76 L/min — 36 ft^3/h), with appropriate trailing shields used for welding Ti-15-3.

Measurements of arc force were also made for an arc maintained between the 2% thoriated tungsten electrode and a water-cooled copper anode. This technique was used to examine the influence of welding current, shielding gas and electrode tip immersion depth on the arc force.

Subsurface GTAW Measurements

After establishing the validity of the arc force measurement technique using surface GTA welding, the effects of the welding current, base metal type, shielding gas and electrode tip immersion depth on the arc force were determined for the subsurface condition. Initial experiments were conducted on a water-cooled copper anode to simulate the influence of arc confinement on the measured arc force in a more controlled manner. The influence of cavity depth on measured arc force was examined by maintaining an arc between the 2% thoriated tungsten electrode and a grooved water-cooled copper anode. Welds were produced at currents of 100, 200 and 300 A, and a constant travel rate of 5.1 mm/s. The groove was 12.7 mm in width and varied in depth (stepped) in increments of 2, 4, 6, 8 and 10 mm (0.08, 0.16, 0.24, 0.31 and 0.39 in.), as schematically shown in Fig. 3A. During the experiment, the distance between the tip of the electrode and the bottom of the groove was maintained at 6 mm. Inert gas shielding was provided by argon at 38 L/min. In a second experiment, the influence of groove width on

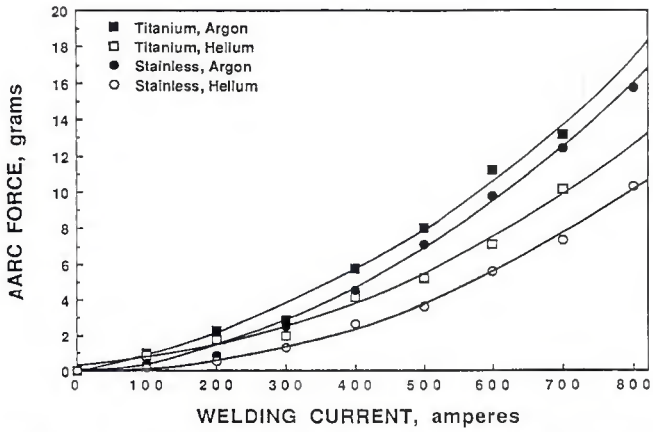

Fig. 4 — Plot of arc force vs. welding current for surface GTA welds produced in titanium and stainless steel. Electrode tip-to-workpiece distance = 6 mm; travel rate = 5.1 mm/s; argon and helium shielding.

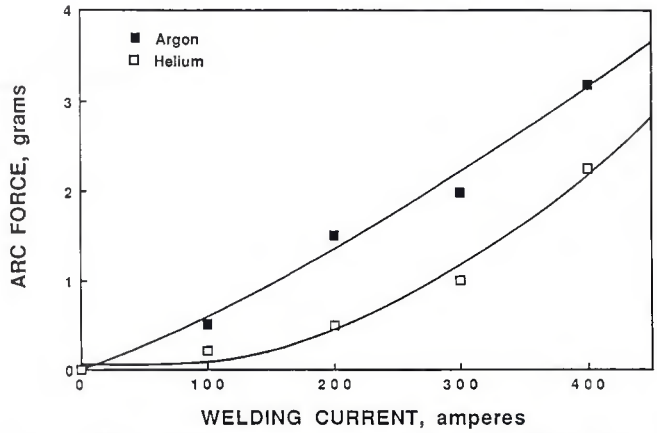

Fig. 5 — Plot of arc force vs. current for arc produced between tungsten electrode and copper anode. Electrode tip-to-workpiece distance = 6 mm; travel rate = 5.1 mm/s; argon and helium shielding.

arc force was determined by continuously decreasing the width of a square groove 6 mm in depth from 32 to 12.7 mm (Fig. 3B). As in the previous experiment, the distance between the tip of the electrode and the bottom of the groove was maintained constant at 6 mm (in other words, the electrode tip-to-workpiece distance was equal to zero).

Subsurface GTA welds were produced in the titanium and stainless steel base materials with electrode tip immersion depths of 0, 2 and 4 mm for titanium only below the plate surface. Welds were initiated in the surface condition (6 mm electrode-to-work distance) and the electrode was slowly lowered in stepped increments, where it remained for sufficient time to reach a quasi-steady-state condition and constant arc force value (generally 5 to 10 s) before lowering to the next level. Welding currents were generally varied from 400 to 900 A in 100-A increments (DC, electrode negative), with the weld travel rate remaining constant at 5.1 mm/s. All welds were bead-on-plate produced autogenously and exhibited partial penetration. As in the surface GTA welds, the exclusive variation of the current and electrode position in these experiments precluded achieving high integrity in all welds.

Weld Characterization

After welding, selected specimens were sectioned, mounted in epoxy, ground, polished and etched for metallographic analysis. Weld penetration depth, surface bead width and the overall weld pool geometry were characterized. In addition, the morphology of the columnar fusion zone grain structure and the cellular-dendritic solidification substructure were analyzed to develop a further understanding of weld pool cavity shape and weld solidification conditions.

Results

Experimental results are presented and discussed in the sections below in order of: 1) arc force measurements for surface GTAW, 2) arc force measurements for subsurface GTAW, and 3) characterization of the weld pool geometry.

Arc Force Measurements for Surface GTAW

Surface GTAW measurements were performed primarily for comparison with previously published values of arc force for surface GTAW and with arc force measurements obtained in this study for subsurface GTAW. Test results for consumable anodes (titanium and stainless steel) and the water-cooled copper anode are presented in Figs. 4 and 5, respectively. Unless noted otherwise, all force measurements presented are "corrected" to give only the arc plasma jet contribution to the total measured force. These corrected arc force values were approximately 50% of the total arc force measured. Similar proportions have been reported by other investigators (Ref. 26). Values of arc force measured for titanium and stainless steel base materials (Fig. 4) and a water-cooled copper anode (Fig. 5) were found to increase parabolically with the welding current, with a maximum arc force of approximately 16 g measured at 800 A for a weld produced in titanium with argon shielding. The results generally compared quite favorably with published data shown in Fig. 2.

In addition to the influence of welding current, the arc force data presented in Figs. 4 and 5 indicate an influence of the base metal substrate and the shielding gas on the arc force. A higher arc force was measured for titanium vs. stainless steel, with the difference being more significant for helium vs. argon shielding. A consistently greater arc force for argon vs. helium shielding is also shown.

Final measurements of arc force for the surface GTAW condition evaluated the influence of electrode tip-to-workpiece distance on measured arc force. Results were consistent with those reported by Savage and coworkers (Ref. 23). Recently, Lin and Eagar (Ref. 21) also showed an increase in maximum arc pressure with a decrease in electrode tip-to-workpiece distance, with the effect most significant for helium shielding. In the present work for stainless steel plate welded at 300 A in argon, the arc force increased from 2.7 g at an electrode tip-to-workpiece distance of 0.25 in. to 4.5 g for a zero gap.

Arc Force Measurements for Subsurface GTAW

Corrected arc force measurements were made for subsurface GTA welds produced on consumable titanium and stainless steel anodes, and on water-cooled copper anodes to simulate geometric containment effects experienced by the arc. Figure 6 shows a plot of arc force vs. the distance between the electrode tip and the top surface of the copper plate for arcs produced between the tungsten electrode and a water-cooled copper electrode that contained a 6-mm- wide square groove which increased in stepped increments from 0 to 10 mm deep. As shown, an increase in the electrode tip immersion depth below the top surface of the plate (while maintaining a constant distance from the electrode tip to the bottom of the groove constant of 6 mm) resulted in a continuous

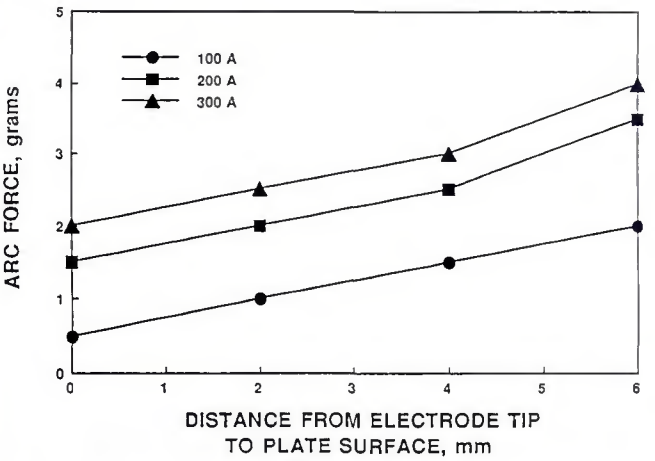

Fig. 6 — Plot of arc force (gm) vs. distance from electrode tip to plate surface (mm) for tungsten arcs produced within 12.7-mm wide groove in water-cooled anode. The distance between the electrode tip and the bottom of the groove was maintained at 6 mm. Travel rate was 5.1 mm/s; argon shielding.

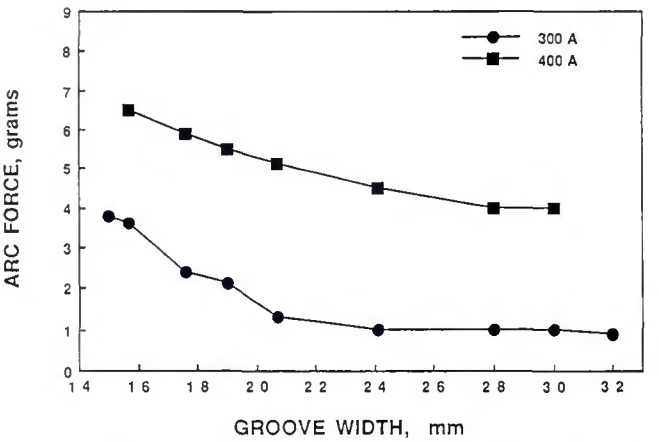

Fig. 7 — Plot of arc force vs. groove width in water-cooled copper anode. Groove depth was 6 mm, and the distance between the electrode tip and the bottom of the groove was maintained at 6 mm. Travel rate was 5.1 mm/s; argon shielding.

increase in arc force for all three currents evaluated. Although not shown in Fig. 6, a further increase in immersion depth above 6 mm (measurements were made at 8 and 10 mm at 300 A) showed no further increase in arc force.

Figure 7 shows the results of a similar analysis in which an arc was maintained between the tungsten electrode and a water-cooled copper anode containing a groove of varying width but with a constant 6-mm depth. For a constant electrode tip-to-groove bottom distance of 6 mm (*i.e.*, zero gap between the electrode tip and the top of the anode), the arc force increased with a decrease in the groove width.

Figures 8 and 9 show plots of arc force vs. welding current for surface GTA welds (6 mm electrode tip-to-workpiece distance) and subsurface GTA welds produced at various electrode tip immersion depths in titanium for argon and helium shielding, respectively. As with the surface measurements, arc force data obtained for all electrode immersion depths consistently showed a parabolic increase in arc force with an increase in welding current. A decrease in the electrode tip-to-workpiece distance to zero and finally to a subsurface condition resulted in an increase in the measured arc force. For welds produced in titanium using argon shielding, an electrode tip immersion of 4 mm resulted in approximately a 25 to 35% increase in arc force vs. the surface condition over a range of welding currents. For helium shielding, an even greater proportional increase in arc force was measured for an electrode tip immersion depth of 2 mm, with nearly a 100% increase vs. the surface arc (6 mm) condition. The influence of shielding gas type on arc force also paralleled the results of surface studies, with argon consistently registering higher arc force levels for comparable electrode tip immersion depths.

Arc force vs. welding current for surface and subsurface GTA welds produced in stainless steel with argon shielding is plotted in Fig. 10 and shows a significant increase in measured arc force with electrode immersion. At a 400-A welding current, the arc force increased from about 4.5 to 12 g in transition from surface condition to a 2-mm electrode tip immersion depth. Although the arc force levels measured for stainless steel were below those of titanium in the surface condition, the greater increase in arc force with immersion for stainless steel resulted in greater measured force levels in the zero gap and 2-mm electrode tip immersion depth conditions.

Weld Pool Geometry

Selected surface and subsurface GTA welds were sectioned for metallographic analysis to better understand how weld-

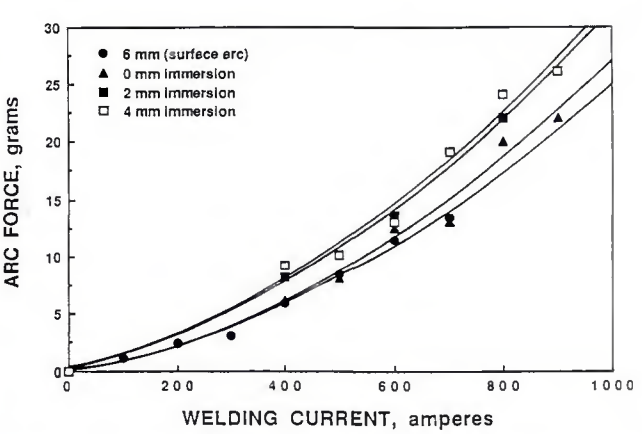

Fig. 8 — Plot of arc force vs. welding current for surface and subsurface GTA welds produced in titanium at varying electrode tip-to-workpiece distances. Travel rate = 5.1 mm/s, argon shielding.

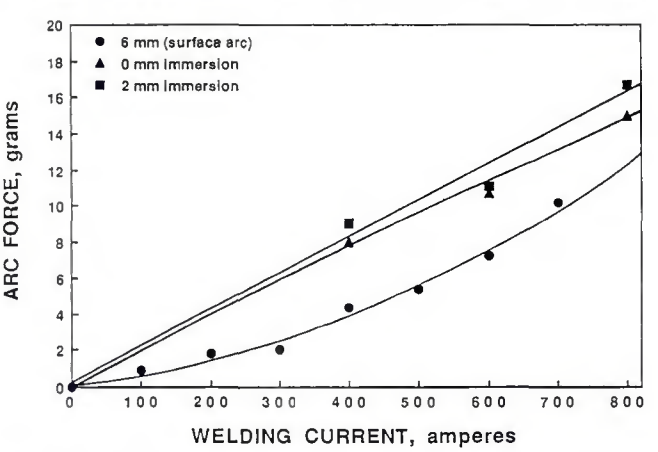

Fig. 9 — Plot of arc force vs. welding current for surface and subsurface GTA welds produced in titanium at varying electrode tip-to-workpiece distances. Travel rate = 5.1 mm/s, helium shielding.

ing parameters (in particular electrode tip immersion depth and shielding gas) influence the geometry of the molten weld pool and the cavity within which the electrode is submerged. Figure 11A–D shows light macrographs of GTA welds produced in the Ti-15-3 titanium plate at a 500-A welding current, 5.1 mm/s travel rate, argon and helium shielding and with electrode tip immersion depths of 0 and 4 mm.

A significant influence of shielding gas on the weld pool geometry and depth-to-width ratio is apparent. Welds produced with argon shielding exhibited two different grain structure patterns. In the lower portion of the weld pool, columnar beta grain solidification occurred epitaxially from the side walls toward the center of the pool, abutting at the weld centerline. The solidification structure resembled that exhibited by titanium alloy welds produced using high-energy-density processes approximating two-dimensional (thin-plate condition) heat flow. Near the top of the weld, the fusion zone broadened and the beta grain growth orientation changed toward the top surface, similar to grain growth in conduction-limited, three-dimensional, heat-flow conditions (similar to a thick-plate condition) commonly observed in partial-penetration surface GTA welds in titanium plate. Despite the surface broadening, depth-to-width ratios of the welds produced in argon were

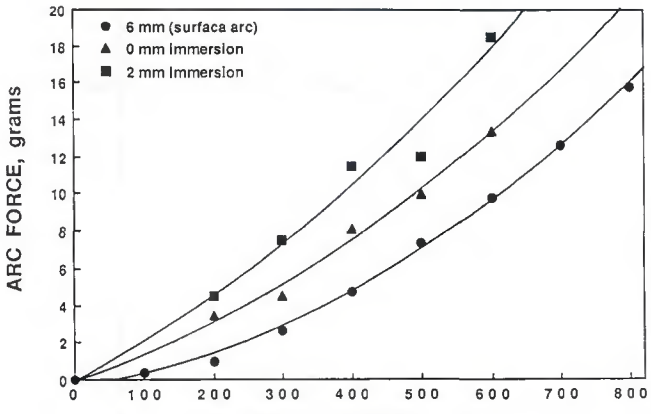

Fig. 10 — Plot of arc force vs. welding current for surface and subsurface GTA welds produced in stainless steel at varying electrode tip-to-workpiece distances. Travel rate = 5.1 mm/s, argon shielding.

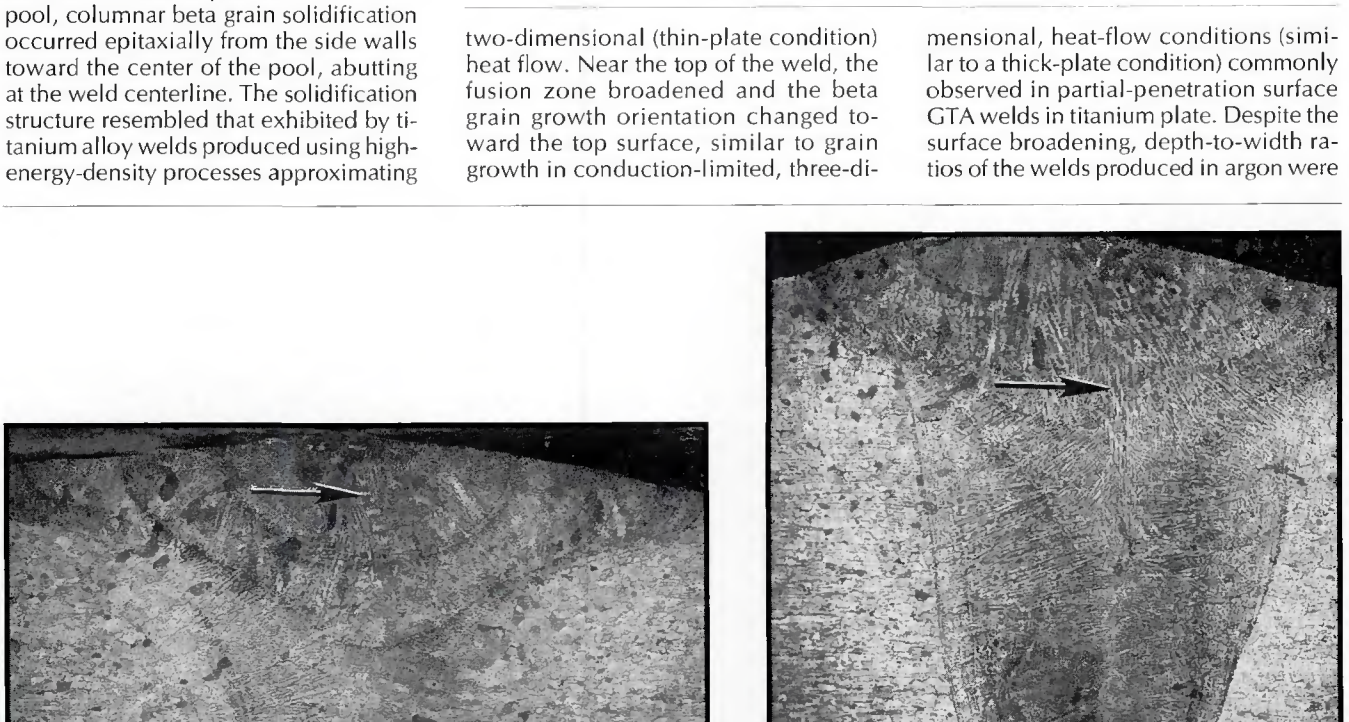

Fig. 11 — Macrographs showing transverse cross-sections of subsurface GTA welds produced in titanium with electrode tip-to-workpiece distances of zero and –4 mm. Arrows indicate approximate location of electrode tip during welding. Welding current = 500 A and travel rate = 5.1 mm/s. A, C — Argon shielding; B, D — helium shielding. Note differences in the growth orientation of columnar beta grains.

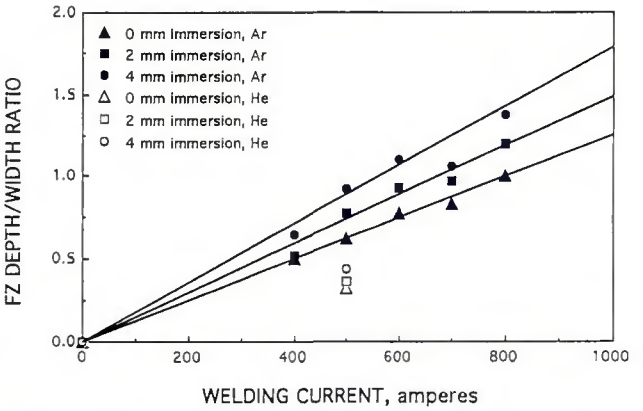

Fig. 12 — Plot of weld fusion zone D/W ratio vs. welding current for surface and subsurface GTA welds produced in titanium at varying electrode tip-to-workpiece distances. Travel rate = 5.1 mm/s, argon shielding.

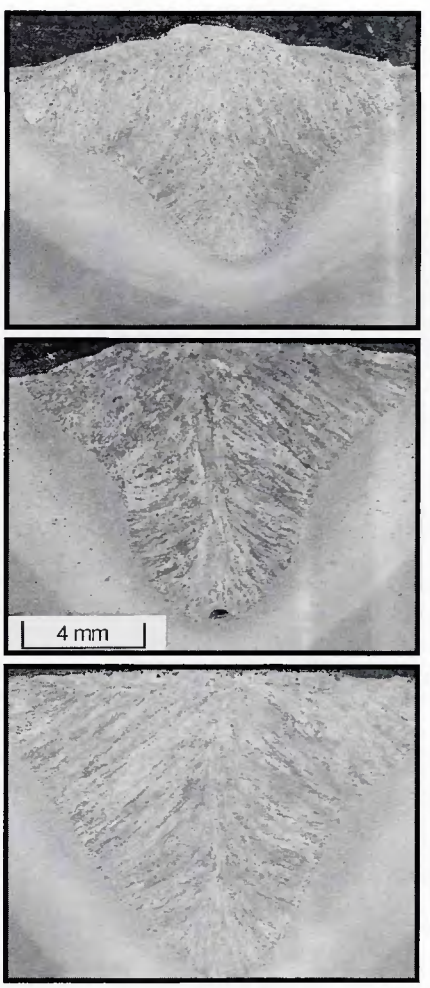

Fig. 13 — Macrographs showing transverse cross-sections of surface and subsurface GTA welds produced in Type 410 stainless steel at electrode tip-to-workpiece distances. Top to bottom: 6 mm, zero, –2 mm. Welding current = 400 A, travel rate = 5.1 mm/s, argon shielding.

0.62 and 0.9 for the weld produced with 0 and 4 mm electrode tip immersion depths. Welds produced with helium shielding using identical parameters (Fig. 11C and D) did not exhibit the region of deep penetration. Instead, they showed shallow, low depth-to-width ratios (0.32 and 0.40 for welds produced with 0 to 4 mm electrode-tip immersion depths, respectively). Solidification occurred in a manner typical of three-dimensional, conduction-limited heat flow, with columnar beta grains growing from the base metal substrate up toward the weld pool surface. The weld produced with a 4-mm electrode tip immersion depth did show evidence of a transition to the deeper penetrating fusion zone geometry exhibited by the argon-shielded welds, and perhaps at higher electrode tip immersion depths would result in the formation of such a weld pool geometry.

Figure 12 shows a plot of weld depth/width ratio vs. welding current for subsurface GTA welds produced in the titanium plate with argon and helium shielding gases, and indicates an increase in this ratio with an increase in welding current and electrode tip immersion depth. Although the data were limited to only one current level, a higher weld depth/width ratio was also observed for argon vs. helium shielding.

The weld fusion zone geometry for surface and subsurface GTA welds produced in Type 410 stainless steel differed from those produced in titanium. As shown in Fig. 13, a decrease in the electrode tip-to-workpiece distance from 6 mm to the subsurface condition of –2 mm promoted an increase in both the depth of penetration and depth-to-width ratio. Columnar grain growth during solidification of the stainless steel welds occurred both in toward the centerline and up toward the top and center of the fusion zone, with the two distinct regions of differing growth orientation observed in the titanium welds produced with argon shielding not apparent. Consistent with the weld macrographs, the weld depth-to-width ratio increased with current level and immersion depth — Fig. 14. Limited data obtained for subsurface GTA welds produced in the stainless steel with helium shielding showed a decrease in the fusion zone depth-to-width ratio vs. welds produced in argon.

Discussion

The section below correlates and further discusses results obtained in this study. Based on the similarities in the relationships observed for the surface and subsurface conditions, parametric effects on arc force, and the origin of these effects, are discussed concurrently for these two conditions in a comparative manner.

Effect of Welding Current on Arc Force

The parabolic relationship measured in the present study between arc force and welding current for both surface and subsurface GTA welding was generally very consistent with that observed by previous investigators for surface welding conditions, and with a recent theoretical analysis by Converti (Ref. 28). As indicated above, the subsurface GTA welds produced using helium shielding did not exhibit a distinct parabolic relationship. However, it is believed that this inconsistency resulted principally from insufficient data obtained from helium-shielded welds required to construct a complete plot rather than from a fundamental change in the phenomena/conditions that control this relationship. Although all arc force data presented in the study were corrected to include only force contributions from the arc plasma jet, an analysis of the uncorrected total arc force levels determined k coefficient values in Equation 1 to be between 5 and 6 X 10^{-6} g/A^2, which are exactly in the range reported by Erokhin's work (Ref. 22). Generally, arc force measurements for surface conditions obtained in the present work fell within the range of plasma jet (*i.e.*, corrected) arc force values reported by several previous investigators (Fig. 2), despite differences in measurement techniques and welding conditions.

Effect of Electrode Tip Immersion Depth on Arc Force

An analysis of the literature reveals very little information regarding the influence of electrode tip-to-workpiece distance on the measured arc force, and no data for the subsurface arc condition. Work by Savage and coworkers (Ref. 23) showed a reduction in the surface arc

length to increase arc force, although his uncorrected arc force measurements were appreciably greater for similar welding parameters than those in the present study. Lin and Eagar (Ref. 21) showed an increase in maximum arc pressure with a decrease in arc length, with the effect appreciably more significant for helium vs. argon shielding gas. They attributed this difference to the greater spreading of the helium plasma jet vs. that of argon, and correspondingly, the higher radial momentum dissipation in helium. Results of the present study were consistent with these previous results in determining that a decrease in the electrode tip-to-workpiece distance in incremental steps from a 6-mm surface condition to a condition in which the electrode tip was immersed 4 mm below the surface of the workpiece showed an increase in arc force for both base metal types and shielding gases.

An analysis of the weld pool geometries and the results of tests performed on water-cooled copper anodes provides some rationale for the observed relationships. The results of experiments on grooved, water-cooled, copper anodes clearly suggest an "arc containment" effect, such that an arc produced within a cavity surrounded by solid metal exerts a greater force than an arc produced (for the same welding parameters and electrode tip-to-workpiece distance) on a flat, open surface. Although not detailed here, the influence of arc containment may be explained using fluid mechanics models relating the influence of surface geometry on changes in the momentum flux of an impinging fluid (Ref. 29). This analysis suggests that changes in the momentum flux of the incoming vs. the outgoing arc plasma jet (after it impinges the surface) is strongly influenced by the surface geometry (*i.e.*, the weld pool surface profile). With the change in momentum flux, therefore, the effective reaction force imparted by the arc plasma jet becomes greater as the surface becomes increasingly convex and deeper. Intuitively, this is the same effect that results in a greater force being produced on a cupped surface impinged by a gaseous or liquid fluid vs. a flat surface of the same projected area. The differences in this force results because the change in momentum of the fluid impinging the surface and being reversed in direction is greater for the convex vs. the flat surface.

This arc containment effect may in part explain the consistently greater arc force measurements for titanium alloy welds produced with argon vs. helium shielding. Based on the analysis of weld pool geometry and columnar beta grain and solidification-substructure orientation, welds produced with argon shielding and an immersed electrode tip condition appeared to exhibit a deep weld cavity and pool shape. In contrast, welds produced in titanium with helium shielding, even with a 4-mm electrode tip immersion depth, exhibited a much shallower and less concave pool surface. This lower degree of arc containment by the welds produced in helium apparently contributed in part to the lower arc force levels.

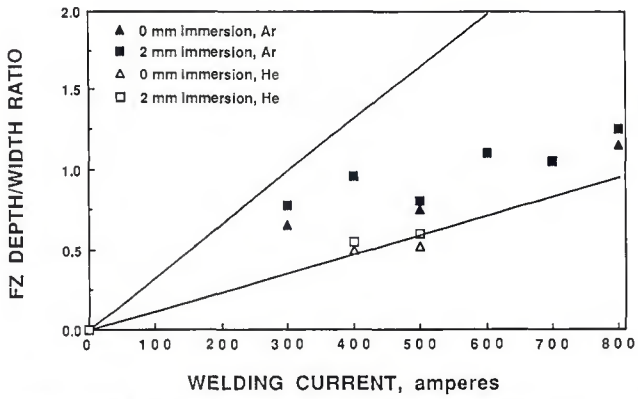

Fig. 14 — Plot of weld fusion zone D/W ratio vs. welding current for surface and subsurface GTA welds produced in stainless steel at varying electrode tip-to-workpiece distances. Travel rate = 5.1 mm/s, argon and helium shielding.

Additional factors may also contribute to an increase in arc force with increased electrode tip immersion. The immersion of the electrode tip within a cavity, in conjunction with a relatively short arc length and high arc current, vaporize elements in the molten weld pool. The presence of these elements in the plasma likely influence the arc plasma geometry and ultimately the arc force.

Effect of Shielding Gas on Arc Force

The higher arc force levels consistently measured for welds produced with argon vs. helium shielding for both surface and subsurface GTAW conditions were consistent with previous arc pressure measurements by Lin and Eagar (Ref. 21) and Yamauchi (Ref. 30). In addition to the aforementioned effect of weld pool surface shape, factors that promote this behavior include the greater density of argon vs. helium, and the higher velocity of the argon vs. the helium arc plasma jet due to the higher viscosity of helium vs. argon (Ref. 21).

As indicated in the previous section, differentiating the influence of shielding gas on arc force in welds produced on actual consumable anodes becomes more complex due to synergism effects. In actual welds, the arc pressure distribution and arc force may be affected by variables other than differences in the physical and electrical properties of the inert gases. These may include the actual arc length, the geometry of the pool surface and weld pool vaporization effects.

Effect of Base Metal Type on Arc Force

The higher arc force values measured for titanium vs. stainless steel base metals under surface conditions were consistent with results previously reported by Burleigh (Ref. 27). He suggested that this difference may originate from differences in the arc plasma composition caused by variations in the level of vaporized metallic elements in the arc, as influenced by differences in the heats of vaporization of these elements. Arc force values for both base metals were well above values measured for the water-cooled copper electrode, further suggesting that base metal vaporization may have affected the arc and ultimately the arc force.

The higher levels of arc force for stainless steel as compared to titanium under identical welding conditions suggest that a different effect begins to dominate the arc force with increased immersion depth.

Effect of Welding Conditions on Weld Pool Geometry

Although the present study was limited with regard to base metal thickness, welding current, and electrode tip penetration (because of limitations of the maximum load capacity of the scale), results clearly showed an influence of increased electrode tip immersion depth on increasing the weld fusion zone penetration and depth-to-width ratio over a wide range of welding currents. For current levels used in the present work, this influence was most significant for argon shielding because of the basic geometry of the weld pool produced.

Conclusions

1) Measurements of the force exerted by the gas tungsten arc on titanium alloy and stainless steel plates for the surface condition have shown a parabolic relationship between the "corrected" arc force and the welding current for cur-

rent levels ranging from 100 to 800 A. For identical welding parameters, arc force levels were greater for titanium than stainless steel and for argon compared to helium shielding.

2) An increase in electrode immersion depth from the surface condition to below the workpiece surface promoted an increase in arc force for both base materials and shielding gases.

3) Subsurface GTA welding experiments on the base materials showed a similar parabolic increase in corrected arc force with welding current, with a maximum arc force of 25 g at 900 A and a submersion depth of 4 mm below the workpiece surface. Arc force measurements were greater for stainless steel than titanium in the subsurface condition, and higher for welds produced with argon vs. helium shielding.

5) Experiments performed using a grooved, water-cooled copper anode indicated an increase in arc force with increased "containment" of the arc within the simulated weld cavity, suggesting that this effect may contribute in part to the greater arc forces measured in the subsurface condition.

6) Weld fusion zone penetration and depth-to-width ratio increased with electrode immersion depth, with the latter being appreciably greater for argon vs. helium shielding. These differences have been attributed in part to different cavity and weld pool geometries for these different shielding gases, and are correlated with differences in measured arc force.

Acknowledgments

The authors thank Miller Electric Mfg. Co., W. Arter of Jetline Engineering and Larry Heckendorn of Toledo Scale for donating equipment to this project. The authors also thank Leon Madrid and Jeff Glazier of The Ohio State University and Ted Widener from Trent Tube, Inc., for their significant technical contributions. Finally, the financial support of The Edison Welding Institute is acknowledged.

References

1. Goryachev, A. P., and Zelenin, V. A. 1964. Mechanized deep penetration arc welding with a tungsten electrode. *Automatic Welding* 17(12):21–26. Translated from *Avt. Svarka.* 1964 (12):24–29 of the Arc Welding Institute, Kiev, published by the Ukrainian SSR Academy of Sciences.

2. Gorshkov, A. I., and Tretyakov, F. E. 1966. Subsurface arc welding of titanium alloy GT6S. *Welding Production* 13(1):47–51. Translation from *Svar. Proiz.* 1966(1):24–26, Mashinostroenie, Moscow.

3. Rabin, D. M. *et al.* 1971. Aluminum alloys welded with DC the electrode negative. *Automatic Welding* 24(3):72–73. Translation from *Avt. Svarka.* 1971(3):71–72 of the Arc Welding Institute, Kiev, published by the Ukrainian SSR Academy of Sciences.

4. Luk'yanenko, V. M., *et al.* 1971. Manufacturing welded hydrolysis apparatus from AZT alloy. *Welding Production* 18(10):71–74. Translation from *Svar. Proiz.* 1971(10):44–45, Mashinostroenie, Moscow.

5. Kudoyarov, B. V., *et al.* 1972. On the connection between the inclination of the welding arc and the formation of gas cavities in a weld. *Welding Production* 19(4):14–17. Translation from *Svar. Proiz.* 1972(4):9–10, Mashinostroenie, Moscow.

6. Demyantsevich, V. P., and Matyukhin, V. I. 1972. Characteristics of the movement of molten metal in a weld pool during welding with a nonconsumable electrode. *Welding Production* 19(10):1–4. Translation from *Svar. Proiz.* 1972 (10):1–3, Mashinostroenie, Moscow.

7. Suzdalev, I. V., *et al.* 1972. Influence of the angle of inclination of the electrode on the formation of gas cavities during argon-arc welding of titanium. *Welding Production* 19(11):75–77. Translation from *Svar. Proiz.* 1972(11):44–45, Mashinostroenie, Moscow.

8. Demyantsevich, V. P., and Matyukhin, V. I. 1972. Distribution of temperature in the molten pool during welding with a nonconsumable electrode and the arc immersed in the work. *Automatic Welding* 25(11):5–7. Translation from *Avt. Svarka.* 1972(11):5–7 of the Arc Welding Institute, Kiev, published by the Ukrainian USSR Academy of Sciences.

9. Demyantsevich, V. P., and Matyukhin, V. I. 1973. Gas shielded arc welding of titanium alloys with the arc immersed in the work with controlled bead shaping. *Welding Production* 20(9):27–30. Translation from *Svar. Proiz.* 1973(9): 16–17, Mashinostroenie, Moscow.

10. Shelenkov, G. M., *et al.* 1974. Tungsten electrodes for submerged arc welding of titanium. *Welding Production* 21(4):36–38. Translation from Svar. Proiz 1974(4):21–23, Mashinostroenie, Moscow.

11. Zemlevskii, L. A., and Leskov, G. I. 1978. Investigation of the melting of the metal during welding with an immersed arc. *Automatic Welding* 31(3):8–10. Translation from *Avt. Svarka.* 1978(3):16–17 of the Arc Welding Institute, Kiev, published by the Ukrainian SSR Academy of Sciences.

12. Simonik, A. G. 1980. The welding of a magnesium alloy with a submerged nonconsumable electrode. *Welding Production* 27(5):17–20. Translation from *Svar. Proiz.* 1980(5): 14–17, Mashinostroenie, Moscow.

13. Simonik, A. G., and Vereschagin, S. I. 1982. Welding with an immersed nonconsumable electrode with control of welding current. *Welding Production* 29(3):13–15. Translation from *Svar. Proiz.* 1982(3):13–14, Mashinostroenie, Moscow.

14. Feingenson, N. B., *et al.* 1982. Effect of welding conditions on weld formation when welding VT20 alloy with an immersed electrode. *Welding Production* 29(11):19–20. Translation from *Svar. Proiz.* 1982(11):17-18 Mashinostroenie, Moscow.

15. Shtrikman, M. M., *et al.* 1973. Steels welded with an immersed arc from a tungsten electrode. *Automatic Welding* 26(8):46–50. Translation from *Avt. Svarka* 1973 (8):50–53 of the Arc Welding Institute, Kiev, published by the Ukrainian SSR Academy of Sciences.

16. Matyukhin, V. I., *et al.* 1974. Characteristics of buried-arc welding of stainless and heat-resistant steels and alloys with a nonconsumable electrode. *Welding Production* 21(9):41–44. Translation from *Svar. Proiz.* 1974(9):24–26, Mashinostroenie, Moscow.

17. Lukens, W. E. 1987. Mechanical properties of buried gas tungsten arc HY-100 and HSLA steel weldments. *Welding Journal* 66(7):215-s to 220-s.

18. Adonyi, Y., Campos, A., and Baeslack, W. A. III. 1988. Submerged-GTA welding of stainless steels. EWI Research Report MR8815, Edison Welding Institute, Columbus, Ohio.

19. Milner, D. R., Salter, G. R., and Wilkinson, J. B.,1960. Arc characteristics and their significance in welding. *British Welding Journal* 7(2):73–78.

20. Wilkinson, J. B., and Milner, D. R. 1960. Heat transfer from arcs. *British Welding Journal* 7(2):115–128.

21. Lin, M. L., and Eagar, T. W. 1986. Pressures produced by gas tungsten arcs. *Metallurgical Transactions* 17B(9):601–607.

22. Erokhin, A. A. 1979. The force exerted by the arc on the metal being melted. *Automatic Welding* 32(7):17–23. Translation from *Avt. Svarka.* (7):21–26 of the Arc Welding Institute, Kiev, published by the Ukrainian USSR Academy of Sciences.

23. Savage, W. F., Nippes, E. F., and Agusa, K. 1979. Effect of arc force on defect formation in GTA welding. *Welding Journal* S8(7):212-s to 224-s.

24. Stolpner, E. A., *et al.* 1971. Procedure for determining the dynamic pressure of pulsed arcs. *Welding Production* (9):12–16. Translation from *Svar. Proiz.* 18(9):8–10, Mashinostroenie, Moscow.

25. Kublanov, V., and Erokin, A. 1974. The arc force on molten metal pools. *Welding Production* 21(5):19–20. Translation from *Svar. Proiz.* 1974(5):11–12, Mashinostroenie, Moscow.

26. Stolbov, V. I. 1974. Pressure of the powerful three-phase arc. *Automatic Welding* 27(8):9–12. Translation from *Avt. Svarka.* 1974(8):11–13 of the Arc Welding Institute, Kiev, published by the Ukrainian SSR Academy of Sciences.

27. Burleigh, T. D. 1980. Measurement of the arc force in GTA welding. Master's Thesis, Department of Materials Science and Engineering. Massachusetts Institute of Technology. Cambridge, Mass.

28. Converti, J. 1981. Plasma jets in welding arcs. Ph.D dissertation, Massachusetts Institute of Technology, Cambridge, Mass.

29 Albertson, M. 1960. *Fluid Mechanics for Engineers.* New York: Prentice-Hall.

30. Yamauchi, N., and Taka, T. 1979. TIG arc welding with hollow tungsten electrodes, IIW Document 212-452-79.